Desalination and Water Treatment
www.deswater.com
doi: 10.1080/19443994.2015.1039600

57 (2016) 10477–10489
May

Taylor & Francis
Taylor & Francis Group

Effect of the operating temperature on hydrodynamics and membrane parameters in pressure retarded osmosis

Khaled Touati[a,*], Fernando Tadeo[a], Christopher Hänel[b], Thomas Schiestel[b]

[a]*Department of Systems Engineering and Automatic Control, University of Valladolid, 47011 Valladolid, Spain, Tel. +34 983423162; Fax: +34 983423161; emails: kha.touati@gmail.com (K. Touati), fernando@autom.uva.es (F. Tadeo)*
[b]*Fraunhofer Institute for Interfacial Engineering and Biotechnology IGB, Nobelstrasse 12, 70569 Stuttgart, Germany, Tel. +49 711970 4401; Fax: +49 711970 4200; emails: christopher.haenel@igb.fraunhofer.de (C. Hänel), thomas.schiestel@igb.fraunhofer.de (T. Schiestel)*

Received 29 September 2014; Accepted 3 April 2015

ABSTRACT

The osmotic energy recovered by pressure-retarded osmosis from flows of different salinities is affected by the temperature, so its effect on hydrodynamic and membrane parameters is studied here. It is shown by models and experimental results that raising the temperature of the solutions leads to a variation in the mass transfer coefficient, the boundary layer, the diffusion coefficient, the solute resistivity, and the permeability, therefore, affecting the water flux. Consequently, the expected power density is improved at high temperatures, although, the salt flux diffusion increases. Laboratory results are presented using solutions at different concentrations and temperatures to validate the analysis.

Keywords: Pressure-retarded osmosis; Hydrodynamics; Osmotic energy; Temperature effects

1. Introduction

Harvesting clean energy to satisfy the ever-growing energy demand of human society is of great importance for the sustainable development of human civilization [1]. Water and energy are inextricably linked and mutually dependent, with each one affecting the other's availability. Pressure-retarded osmosis (PRO) is one of the processes that shows the strong link between water and energy [2]. The PRO process uses the osmotic pressure as a driving force to produce power. The first exploitations of osmotic power via PRO processes were carried about 40 years ago [3]. This is achieved by an asymmetric membrane separating two streams with different salinity. Water molecules are spontaneously transported through a semipermeable membrane, from a low salinity stream (such as river water, brackish or wastewater), at ambient pressure, to a pressurized high salinity stream (seawater or brine), with the aid of the osmotic pressure gradient across the membrane [4]. The diluted draw solution, with a greater volume and/or pressure, moves a turbine to produce electricity [5]. To make a PRO plant commercially viable, a power density higher than 5 W/m^2 is required [6].

The potential for energy extraction from this "salinity potential" resource (for all river effluents combined) amounts to around 2.4/2.6 TW, close to present day global electricity consumptions [7]. Hopefully, PRO systems will become an effective form of power production in the future, alongside other established renewable technologies (e.g. solar and wind)

*Corresponding author.

[7]. However, several challenges have already been identified, especially concerning membrane development [8].

During the last few decades, some laboratory experiments have shown that PRO performance is affected by the operating pressure, the characteristics of the draw and feed, and the membrane [6,8,9]. Many papers have studied these parameters in great detail. However, few existing publications have focused on the impact of temperature [10]. Like any other membrane processes, temperature should play a significant role in the performance of the PRO process, as it has a direct influence on the thermodynamic properties of both the draw and the feed solutions. In this paper, the effect of the temperature on the solutions and the membrane parameters is studied. Results provided by this study give interesting perceptions to the PRO operating conditions and membrane preparation.

2. PRO background

In PRO, feed and draw solutions are separated by a semipermeable membrane; so water spontaneously permeates through the membrane from the feed to the draw solution, driven by the osmotic pressure difference across the membrane [4]. The ideal osmotic process can be described by the thermodynamic equations for the water and salt fluxes. The general equations of transport are [11]:

$$J_w = A(\Delta\pi_m - \Delta P) \tag{1}$$

$$J_s = B(C_{D,m} - C_{F,m}) \tag{2}$$

where J_w is the water flux, J_s is the salt flux, A is the water permeability coefficient of the membrane, B is the salt permeability coefficient of the membrane, $C_{D,m}$ and $C_{F,m}$ are the solute concentrations at the interface of the active and support layers, respectively, $\Delta\pi_m$ is the difference between osmotic pressures at the surface of the active layer, and ΔP is the hydraulic pressure applied on the draw water side. A schematic of the salt concentration profile across a membrane operating in PRO mode (active layer facing the draw solution) is shown in Fig. 1.

With the use of an asymmetric membrane, internal concentration polarization (ICP) occurs in the porous layer of the membrane, which reduces the osmotic driving force across the active layer, and thus the water flux. In PRO, the orientation of the active dense layer facing the draw solution (AL-DS) is considered to be mechanically more stable, as the external hydraulic pressure is applied on the draw side [12,13]. In this case, concentrative ICP occurs in the porous layer of the membrane.

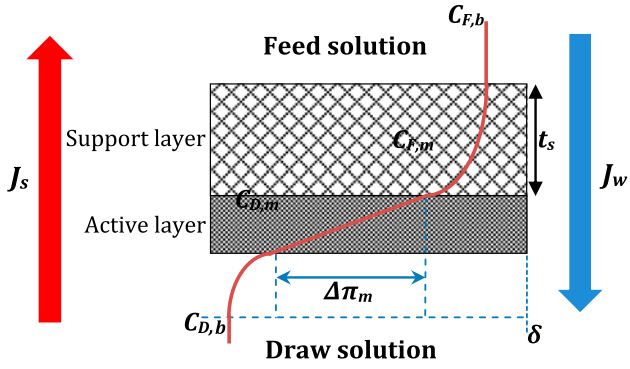

Fig. 1. Schematic representation of the salt concentration profile and water fluxes across a membrane in PRO at steady state.

Due to the ICP within the porous support, reverse salt permeation across the membrane, and the external concentration polarization (ECP) in the draw solution, the effective osmotic driving force is lower than the osmotic pressure difference between the bulk draw and feed solutions. Thus, a more realistic water flux expression is:

$$J_w = A(\pi_{D,m} - \pi_{F,m} - \Delta P) \tag{3}$$

where $\pi_{D,m}$ and $\pi_{F,m}$ are the osmotic pressures at the surface of the active and support layers, respectively. Taking into consideration the effect of ICP and ECP on the driving force, and assuming that the osmotic pressure is proportional to the concentration and the temperature ($\pi = \beta CRT$), the water flux expression is given by [4]:

$$J_w = A\left[\frac{\pi_{D,b}\,\exp\left(\frac{-Jw}{k}\right) - \pi_{F,b}\exp(J_w K)}{1 + \frac{B}{J_w}[\exp(J_w K) - 1]} - \Delta P\right] \tag{4}$$

where $\pi_{D,b}$ is the bulk osmotic pressure of the draw solution near the surface of the active layer, $\pi_{F,b}$ is the bulk osmotic pressure of the feed solution near the surface of the support layer, β is the van't Hoff

coefficient, R is the universal gas constant, and T is the absolute temperature. The mass transfer coefficient (k) is defined as [7]:

$$k = \frac{ShD}{d_h} \tag{5}$$

where D is the diffusion coefficient of the solute in the draw solution, Sh is the Sherwood number, and d_h is the hydraulic diameter of the flow channel defined as:

$$d_h = \frac{4S}{P_w} \tag{6}$$

where S is the area of the flow section and P_w is the hydrated perimeter. For a flat channel with spacer, the hydraulic diameter is [14]:

$$d_h = \frac{4\varepsilon}{\frac{2}{h_{sp}} + (1-\varepsilon)S_{vsp}} \tag{7}$$

where h_{sp} is the thickness of the spacer, S_{vsp} the specific surface of the spacer ($S_{vsp} = S_{sp}/V_{sp}$, with S_{sp} is the surface area of the spacer and V_{sp} the volume of the spacer), and ε the porosity.

The solute resistivity K is defined as [15]:

$$K = \frac{\tau t_s}{\varepsilon D} = \frac{s}{D} \tag{8}$$

where τ, t_s, and s are, respectively, tortuosity, thickness, and structure parameter.

The specific salt flux in PRO, defined as the ratio of salt flux to water flux, J_s/J_w, is affected by the intrinsic transport properties of the membranes, as follows [16]:

$$\frac{J_s}{J_w} = \frac{B}{A\beta RT}\left(1 + \frac{A\Delta P}{J_w}\right) \tag{9}$$

where β is the van't Hoff coefficient, R is the universal gas constant, and T is the absolute temperature.

3. Experimental

3.1. Membranes

Results from experiments with a cellulose acetate flat-sheet PRO membranes (IGB membrane) developed by Fraunhofer Institute for Interfacial Engineering and Biotechnology discussed in Section 5.1 are used. Parameters used for the calculations are summarized in Table 1.

3.2. PRO bench scale

A schematic diagram of the laboratory scale unit used in this study is provided in our previous publication [17]. The test unit had a channel on the feed side of the membrane to allow the feed solution to flow tangentially to the membrane. Mesh spacers placed in the feed channel supported the membrane. A high-pressure positive displacement pump was used to recirculate the feed solution at selected velocities. Purge was collected in a container. Each container was placed on an analytical balance. Temperature was maintained constant using a thermostatic

Table 1
Membrane characteristics

Parameter	Values
Water permeability coefficient A	1.06×10^{-12} m/s/Pa (at 20°C)
Salt permeability coefficient B	2.62×10^{-8} m/s (at 20°C)
Porosity of the support layer ε	80%
Thickness of the active layer e	100 nm
Thickness of the support layer t_s	12 μm
Length of the channel	0.17 m
Effective surface of the membrane	0.013 m^2
Depth of the channel	0.007 m
Width of the channel	0.07 m
Hydraulic diameter d_h	9.4×10^{-4} m
Flow velocity u_0	0.0107 m/s
Structure parameter $s = \tau t_s/\varepsilon$	5.06×10^{-4} m

bath for each bulk. The temperature of the solutions was controlled by electronic thermometer for each side. The flux through the membrane was calculated based on the change in weight of fluids in the graduated containers. The salt flux was determined based on conductivity measurements.

3.3. Chemicals

The feed and draw solutions were prepared using certified ACS-grade NaCl (Fisher Scientific). Osmotic pressures, viscosities, and diffusion coefficients of solutions were calculated using the equations developed in the current study.

4. Effect of the operating temperature on the feed and draw solution chemistry

4.1. The osmotic pressure

The difference in osmotic pressure between bulks is an important parameter in PRO; in fact, the difference in osmotic pressure over the active layer is the effective high driving force of the process, which is affected by the osmotic pressures in the bulks. The feed solution concentration is in general assumed to have a very low concentration, whereas the draw water solution has a high concentration, so as to achieve an appropriate difference of values between the osmotic pressures.

The temperature has a significant impact on the thermodynamic properties of the water. In fact, referring to the van't Hoff equation ($\pi = \beta CRT$), the osmotic pressure is directly proportional to the temperature. It should be pointed out that, the osmotic pressure is not proportional to the concentration for solutions with a very high concentration; however, the assumption of proportionality between the osmotic pressure and the temperature is still applicable: for example, following the results in [18], the expression of the osmotic pressure at a given temperature T, as a function of the concentration C for a NaCl solution can be approximated by:

$$\pi = T_R(3.805C^2 + 42.527C + 0.434) \quad (10)$$

where T_R is the normalized temperature:

$$T_R = \frac{T}{273.15} \quad (11)$$

For simplicity sake, NaCl solutions are now considered; Fig. 2 shows the expected effect of the temperature on the osmotic pressure of the draw solution for different concentrations.

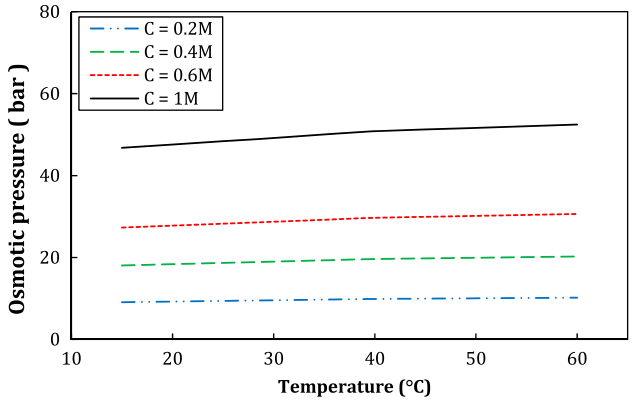

Fig. 2. Osmotic pressure of NaCl solution at different temperatures and concentrations following Eq. (10).

It can be seen that the osmotic pressure increases when the temperature of the solution increases. However, the effect of the temperature on the osmotic pressure is more significant when the concentration of the water is more important: when the concentration is 0.2 M, the pressure gain is around 1.5 bar when the temperature is raised from 15 to 60˚C; whereas the gain is around 7 bars for 1 M. Referring to Eq. (1), as the water flux through the membrane is proportional to the difference of osmotic pressures, then, using a high temperature clearly leads to a better driving force to the process. In PRO processes, the driving force is directly related to the draw solution concentration, which explains the enhanced water flux at higher draw solution concentrations. It is clear that much higher power density can be obtained using brines of high osmotic pressures (such as seawater RO brine, MED brine, and the Dead Sea water) [19].

4.2. The diffusion coefficient D

The diffusion coefficient (D) is an important parameter in PRO as the mass transfer of feed solution (k) and solute resistivity (K) are proportional to D. This coefficient has a strong dependence on the temperature and the concentration of the solution. This diffusion coefficient can be calculated empirically using the Stokes–Einstein relationship [20]:

$$D = \frac{k_b T}{6\pi r \rho \mu} \quad (12)$$

where k_b is the Boltzmann constant, μ is the kinematic viscosity of the NaCl solution, T is the temperature of

the solution, r is the ion radius, and ρ is the density of the solution.

The empirical equations have been proposed to estimate the kinematic viscosity as [21]:

$$\frac{\mu}{\mu_w} = 1 + eC_S \exp\left(\frac{C_S^f}{gT_R + i}\right) \quad (13)$$

where μ_w is the water's kinematic viscosity at temperature T, where $e = 0.12$, $f = 0.44$, $g = 3.713$, and $i = 2.792$ are the fitting parameters (values given for NaCl solutions), and C_S is the molar concentration.

The temperature also affects the dynamic viscosity η. For example, this dependence was described in [22] for NaCl solutions as follows:

$$\eta(T) = 2.414 \times 10^{\left(\frac{247.8}{T - 140} - 5\right)} \quad (14)$$

Using Eqs. (12)–(14), Fig. 3 shows the effect of temperature on the diffusivity of the water through the membrane. It can be seen that in the range of temperature studied, the value of the diffusion coefficient is almost tripled. At low temperatures (from 15°C to 20°C), the effect of the solution concentration on the diffusivity is not significant, as compared to high temperatures, where it becomes more considerable. This is due to the fact that in the NaCl solutions attractive interactions between particles take place, so when the temperature goes up, the viscosity of the solution decreases as the interaction between the particles is reduced due to thermal agitation. Thus, the diffusion coefficient tends to decrease as concentration increases.

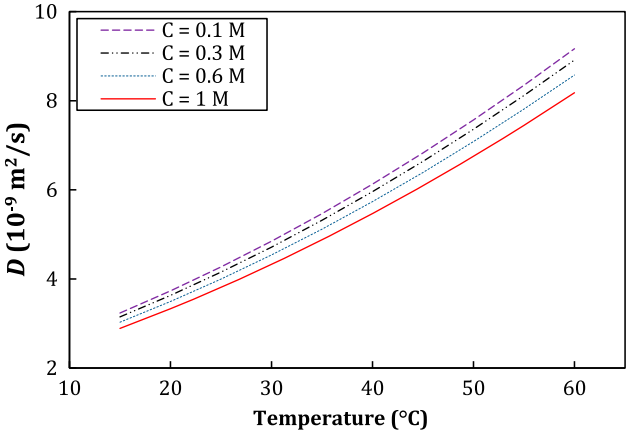

Fig. 3. Diffusion coefficient of NaCl solutions at different temperatures and concentrations.

5. Effect of the operating temperature on the hydrodynamics parameters

5.1. Reynolds, Schmidt, and Sherwood numbers

The mass transfer coefficient (k) depends on the relevant physical properties of the fluid, the geometry used along with relevant dimensions, and the average velocity of the fluid if we are considering flow in an enclosed conduit, or the approach velocity if the flow is over an object. Dimensional analysis can be used to express this dependence in dimensionless form. The dimensionless version of the mass transfer coefficient is the Sherwood number (Sh). The Sherwood number depends on the Reynolds number (Re), and the Schmidt number (Sc). Generally, the flow is considered to be laminar in small pipes and low flow velocities ($Re < 2{,}100$). In several publications, operating in PRO mode, the Sherwood number is determined using the correlation under different flow conditions as [23]:

$$Sh = 0.04\, Re^{0.75}\, Sc^{0.33} \quad \text{(Turbulent flow)} \quad (15)$$

$$Sh = 1.85\left(Re \cdot Sc \frac{d_h}{L}\right) \quad \text{(Laminar flow)} \quad (16)$$

These empirical Sherwood relations are derived from experimental results obtained from UF and RO experiments correlated to the frictional factor of each membrane [24]. However, the structure of PRO membranes is quite different from RO and UF membranes. In fact, the RO membrane support layer is much thicker than the PRO support layer, and UF membranes are considered as porous structure, with higher roughness than PRO membranes. Thus, the use of Eqs. (15) and (16) seems to be inadequate for PRO tests. Moreover, for laminar flow, Eq. (16) is valid where the channel length is significantly larger than hydrodynamic flow development length. In other words, the mass transfer coefficient (k) is valid when the length of the developing region is not significant. However, in lab-scale PRO test, this condition is not valid due to the fact that the channel length is considered in the calculations. In fact, in PRO bench scale, the geometry of the pipes and the low velocity used leads to operation under laminar flow regime. However, PRO membranes are assisted by feed

spacers to maintain the feed channel geometry and to improve mass transfer near the membrane surface. A recent study [25] showed that the use of a spacers-filled flow channel induces a turbulent flow near the membrane surface at low Reynolds numbers. Consequently, the Sherwood number was described in [25] as:

$$Sh = 0.2\,Re^{0.57}\,Sc^{0.4} \tag{17}$$

In Eq. (17), *Re* and *Sc* numbers are assumed to be homogenous over the length of the membrane. In addition, the correlation model depends on the geometry of the spacer used. However, the pressure applied in PRO mode might modify the geometry near the membrane surface, which means that the *Re* and *Sc* are no longer considered homogenous.

Therefore, we proposed to use local values of the Reynolds and Sherwood numbers to estimate the mass transfer across the boundary layer. An exact solution to calculate the local Sherwood for the hydrodynamic boundary layer of a fluid that flows parallel to a smooth, flat, and non-porous surface is developed in [26]. The correlation is described as follows:

$$Sh_x = 0.332\,Re_x^{0.5}\,Sc^{0.66} \quad (\text{Laminar flow for } Re_x < 2.10^5) \tag{18}$$

$$Sh_x = 0.0292\,Re_x^{0.8}\,Sc^{0.66} \quad (\text{Turbulent flow for } Re_x > 2.10^5) \tag{19}$$

The local Reynolds number and the Schmidt number are calculated as follows [27]:

$$Re_x = \frac{u_0 \rho x}{\mu} = \frac{u_0 x}{\eta} \tag{20}$$

$$Sc = \frac{u_0}{\rho D} \tag{21}$$

where u_0 is the velocity of the water, x is the distance from the start of the boundary layer (see Fig. 5), ρ is the density of the water, η the dynamic viscosity of the fluid, μ is the cinematic viscosity, and D is the diffusion coefficient, calculated as shown in Eq. (12).

As shown in Eqs. (20) and (21), the dimensionless numbers Re_x and *Sc* depend on parameters which also depend on the temperature, such as the viscosities μ and η, and the diffusion coefficient (D). Fig. 4 shows the variation of the dimensionless parameters *Re*, *Sc*, and *Sh* with the temperature. Table 2 presents the parameters used for calculations for 1 M NaCl solution. It can be seen that the increase in the temperature leads to an increase in the local Reynolds number regardless of the concentration of the solutions. Moreover, the local Reynolds number exceeds the critical value ($Re_x > 2 \times 10^5$) for a temperature value around 30˚C, which means that the regime of the flow changes from laminar to turbulent. This result is well seen in Fig. 4(c) where an inflection point of the curves is observed for temperatures around 30˚C. As shown in Fig. 4(b), the effect of the concentration on *Sc* is negligible at high temperatures, which is due to the inverse of the diffusivity ($1/D$) present in Eq. (21).

Contrary to the *Sc* number, the concentration effect seems to be insignificant at low temperatures for the local Reynolds number. Raising the temperature of the process leads to the modification of the flow regime from laminar to turbulent because of the strong effect of the temperature on the Re_x value. This leads to enhancement of the mass transfer coefficient (k); therefore, the effect of the ECP is also reduced. Using NaCl solutions, the effect of the concentration is not significant. In fact, the variation of the viscosity and density of the water, within the range of concentrations studied, was not quite important as to affect the local *Re*. For real salty fluids (seawater, brine wastewater, etc.), the result should be similar, due to the fact that the local Reynolds number is not strongly affected by the concentration, as shown in Fig. 4(a). However, the matrix complexity of real fluids can affect the viscosity. For seawater and brine, these effects should be negligible, due to the fact that more than 75% of the matrix is NaCl; however, for wastewater, the composition of the matrix is generally uncontrollable as it contains organic matter, dissolved polymeric waste, etc., which strongly affect the viscosity of the flows and their velocities.

Table 2
Characteristics of 1 M NaCl draw solution at different temperatures

T (˚C)	u_0 (m/s)	ρ (kg/m^3)	μ (m^2/s) × 10^{-6}
20	0.0107	1,042.8	1.095
30	0.0107	1,039.4	0.875
40	0.0107	1,035.5	0.718
50	0.0107	1,030.9	0.602
60	0.0107	1,025.9	0.515

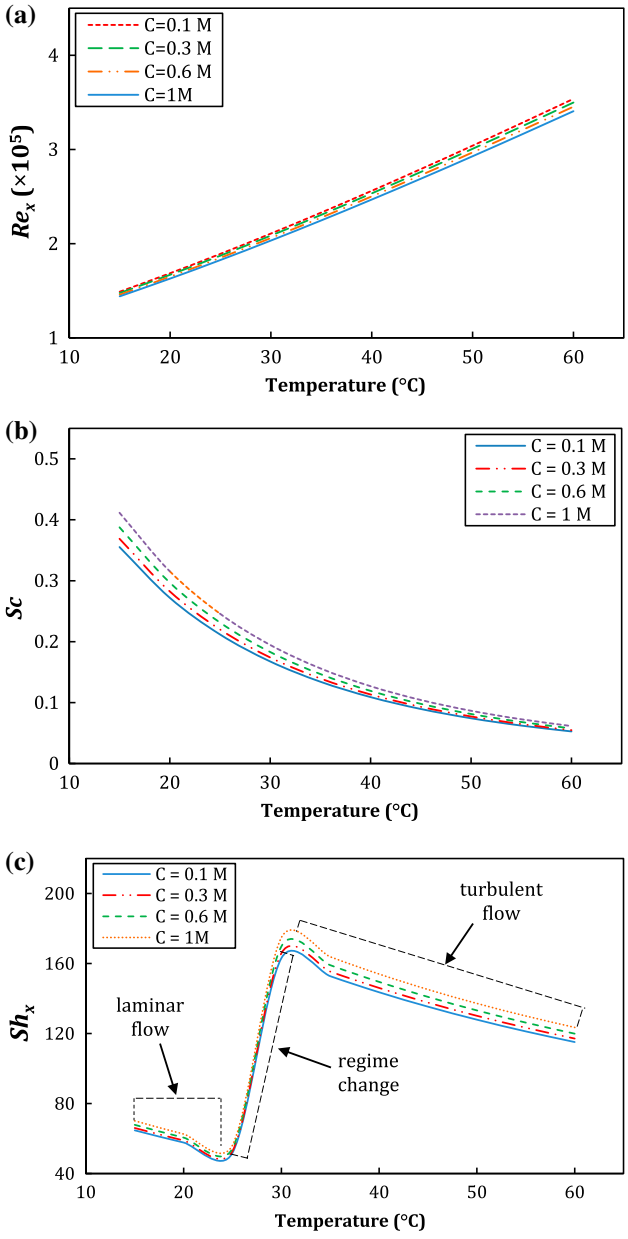

Fig. 4. (a) Reynolds, (b) Schmidt, and (c) Sherwood numbers of NaCl solutions at different temperatures, following Eqs. (18)–(21).

5.2. The boundary layer thickness δ

It is well known that when a viscous fluid flows along a fixed impermeable wall or past the rigid surface of an immersed body, the velocity at any point on the wall or other fixed surface is zero. The extent to which this condition modifies the general character of the flow depends upon the value of the viscosity. If the body is of a streamlined shape, and if the viscosity is small, the effect appears to be confined within narrow regions adjacent to the solid surfaces (the so-called boundary layer). A boundary layer may be laminar or turbulent. A laminar boundary layer is one where the flow takes place in layers, each layer sliding past the adjacent layers. These are found only when the Reynolds numbers are small. A turbulent boundary layer, on the other hand, is marked by mixing across several layers. Thus, there is an exchange of mass, momentum, and energy on a much bigger scale as compared to a laminar boundary layer. A turbulent boundary layer is only obtained at large Reynolds numbers. Eqs. (22) and (23) describe the thickness of the boundary layer for different flow regimes [27]:

$$\delta = \frac{4.91x}{\sqrt{Re_x}} \quad \text{(Turbulent flow)} \tag{22}$$

$$\delta = \frac{0.382x}{(Re_x)^{\frac{1}{5}}} \quad \text{(Laminar flow)} \tag{23}$$

where the distance x is along the membrane (see Fig. 5). It has been shown in [27] that, when the thickness of the boundary layer is smaller, the mass transfer is more important.

The effect of the temperature on the thickness of the boundary layer was studied. Two specific values of x were studied ($x = L$ and $= L/2$). Fig. 6 shows that the effect of the concentration is not really comparable to the effect of the temperature on the boundary layer thickness. The parameter δ has an important dependence on the regime of the flow: a laminar boundary layer is thicker than a turbulent one, thus, which means that the mass transfer behaviors across each layer are not similar. The boundary layer is comparable

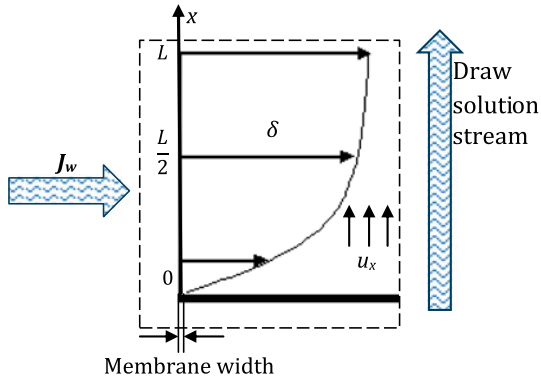

Fig. 5. Schematic of the boundary layer at the draw solution side.

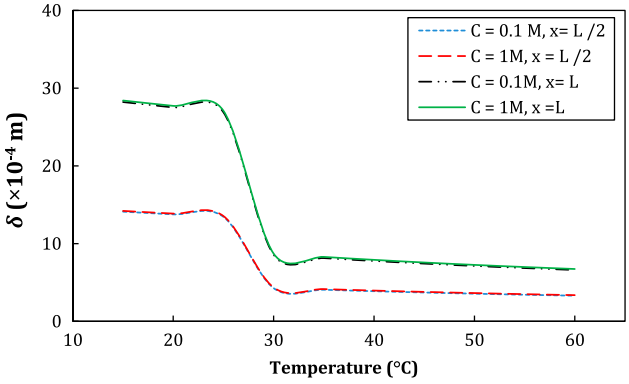

Fig. 6. Thickness of the boundary layer for NaCl solutions at different temperatures, following Eqs. (20), (22), and (23) (u_0 = 0.0107 m/s and L = 0.17 m).

to "a resistance layer" that prevents the passage of the solute to the surface of the active layer, which induces the ECP. With turbulent flow, this resistance is mitigated by the decrease in the boundary thickness. According to Fox et al. [28], ECP is characterized by its modulus $C_{D,m}/C_{D,b} = \exp(-J_w/k) = \exp(-J_w\delta/D)$. Consequently, the decrease of δ induces the increase of k, which drives the concentration value $C_{D,m}$ closer to that of $C_{D,b}$. The viscous effects are not as important at the front of the boundary layer, but become much more important near the end of it. Thus, when the temperature of the water becomes important, the viscosity of the solution is reduced, which leads to an increase in the value of the Reynolds number.

In summary, the increase of in the operating temperature leads to a thinner boundary layer and a higher mass transfer across it.

5.3. Effect of the temperature on the mass transfer coefficient k

The process of mass transfer across an interface in the bulk of a phase is the result of a chemical potential driving force, which is usually expressed in terms of concentrations of the species. The rate of transfer of a given species per unit area normal to the interface, i.e. the flux, depends on some of the physical properties of the system and on the degree of turbulence of the phases involved. As the relationship between the flux and these parameters is not easily developed from fundamentals of mass transfer, coefficients have been defined that lump them all together. These relations are of the form: flux = coefficient × (concentration difference) [29].

In the PRO case, the mass transfer coefficient (k) characterizes the transport of water from the feed solution to the draw solution through the active layer. The mass transfer coefficient described in Eq. (5) depends on parameters that also depend on the temperature. In this section, the effect of the temperature on the mass transfer coefficient is studied experimentally. Four draw solutions with different concentrations were tested (0.1, 0.3, 0.6, and 1 M of NaCl). The local mass transfer coefficient (k_x) can be described using Eqs. (18) and (19) as follows:

$$k_x = \frac{0.332\, Re_x^{0.5}\, Sc^{0.66}}{d_h} D \quad \text{(Laminar flow)} \tag{24}$$

$$k_x = \frac{0.0292\, Re_x^{0.8}\, Sc^{0.66}}{d_h} D \quad \text{(Turbulent flow)} \tag{25}$$

The overall mass transfer coefficient k_{overall} can be calculated by the integration of Eqs. (24) and (25) along the membrane. Thus, k_{overall} is described as:

$$k_{\text{overall}} = \frac{0.332\, Sc^{0.66}}{d_h} D \int_0^L Re_x^{0.5}\, \mathrm{d}x = \frac{0.664\, Re_L^{0.5}\, Sc^{0.66}}{d_h} D \quad \text{(Laminar flow)} \tag{26}$$

$$k_{\text{overall}} = \frac{0.0292\, Sc^{0.66}}{d_h} D \int_0^L Re_x^{0.8}\, \mathrm{d}x = \frac{0.0365\, Re_L^{0.8}\, Sc^{0.66}}{d_h} D \quad \text{(Turbulent flow)} \tag{27}$$

where Re_L is the local Reynolds number at $x = L$.

From Fig. 7, it can be seen that the mass transfer coefficient is drastically affected by the temperature. In fact, when the flow is considered laminar, the effect of the temperature is insignificant in the range of the temperature between 15 and 25°C. However, the behavior of k_{overall} changed drastically above 30°. This result is due to change of the flow regime from laminar to turbulent. As shown in Sections 4.2 and 5.1, the increase in the temperature leads to a decrease in the boundary layer thickness and an increase in the diffusivity: thus the mass transfer increases. In fact, according to film theory, a high diffusivity with a thin boundary layer enhances the rate of mass transfer [30].

At low temperatures, the effect of the concentration on (k_{overall}) is negligible, and seems to be significant at high temperatures. This behavior is similar to that of

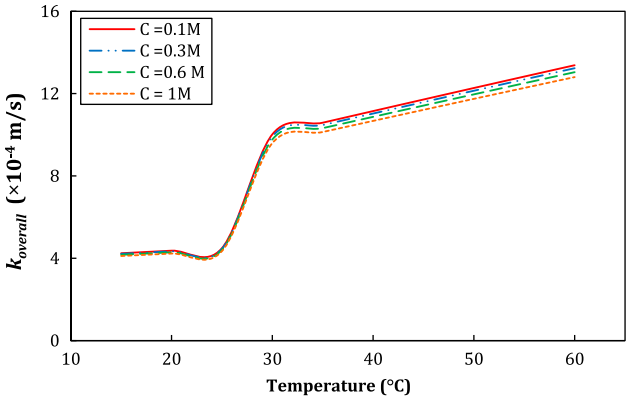

Fig. 7. The overall mass transfer coefficient ($k_{overall}$) for NaCl solutions at different temperatures, following Eqs. (26) and (27).

previously seen in the study of the diffusion coefficient D. Consequently, operating at high temperature can reduce the effect of the ECP by "pushing" $C_{D,m}$ to a value close to $C_{D,b}$.

6. Effect of the operating temperature on the membrane parameters

6.1 Effect of the temperature on the solute resistivity K

The solute resistivity (K), described in Eq. (8), is a parameter used to determine the influence of the ICP on the water flux. Smaller (K) value means less ICP, resulting in higher pure water flux. To determine K experimentally for different operating temperatures, a rearrangement of Eq. (4) was used, as shown below:

$$K = \frac{1}{J_w} \ln\left(\frac{\pi_{D,b} \exp\left(J_w/k\right) + \frac{J_w - B}{A} + \Delta P\left(1 - \frac{B}{J_w}\right)}{\pi_{F,b} + B\left(\frac{1}{A} + \frac{\Delta P}{J_w}\right)}\right) \quad (28)$$

Experimental results were carried out for two draw solutions (0.6 and 1 M of NaCl) and one NaCl feed solution (8.55 mM). The parameters were calculated using experimental results, performed in the range of temperatures from 20 to 60°C. The applied pressure is $\Delta p = 10$ bars. A and B are considered variables with the temperature and their values were taken from our previous work in [17]. The osmotic pressures were calculated using Eq. (10). τ, t_s, and ε are presented in Table 1, and the diffusion coefficient (D) is given by Eq. (12).

Fig. 8 shows the variation of K under different temperatures, where K is firstly calculated using Eq. (8) (lines), and then using Eq. (28) (symbols). It can be seen that, at low temperature, K calculated using Eq. (8) is quite higher than that of Eq. (28) for both tested concentrations. This result might be attributed to the effect of the pressure. In fact, Eq. (8) does not take into consideration the effect of the applied pressure on the support layer. It was shown previously in [31] that, for a given temperature, the increase in ΔP reduces the structure parameter $s = KD$. In our case, two parameters are considered; the temperature and the pressure. Fig. 8 reveals that, at low temperatures, K is high, and the effect of the concentration of the draw solution on K is clearly considerable. In fact, Eq. (28) shows that K is inversely proportional to the water flux of the membrane, so to reach the best performance, the solute resistivity should be as low as possible. Fig. 9 shows the variation of the water flux with the solute resistivity. The modeled J_w (line) is obtained by fitting Eq. (4) using experimental results of K taken from Fig. 8, A and B values from Table 3, and k values taken from Fig. 7. It can be seen that the solute resistivity tends to reduce the water flux of the process: when K is high, the water flux is significantly smaller. In fact, K depends on the structure parameter s: when s decreases, K decreases too, due to the fact that the membrane becomes thinner when the operating temperature increases. This is due to the simultaneous effect of the temperature and pressure: the increase in the operating temperature makes the membrane polymer softer, so tangential forces caused by the applied pressure reduce s. Thus, to reduce the effect of K on the water flux of the membrane and thus on the energy produced using PRO, it would be better to operate with a high temperature, following the results shown in Figs. 8 and 9.

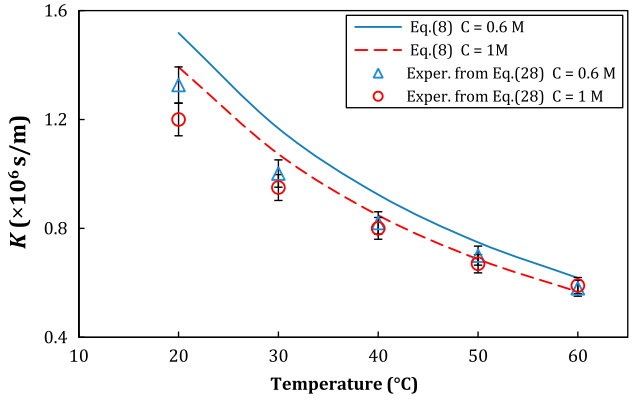

Fig. 8. The solute resistivity (K) for NaCl solutions at different temperatures and concentrations. K is calculated using Eq. (8) (lines), and Eq. (28) using experimental data (symbols).

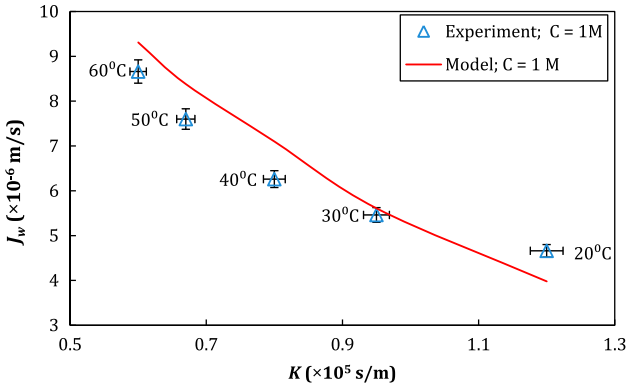

Fig. 9. Modeled (line) and experimental results (symbols) of the water flux J_w with the solute resistivity K ($C_{D,b}$ = 1 M, $C_{F,b}$ = 8.55 mM, and u_0 = 0.0107 m/s).

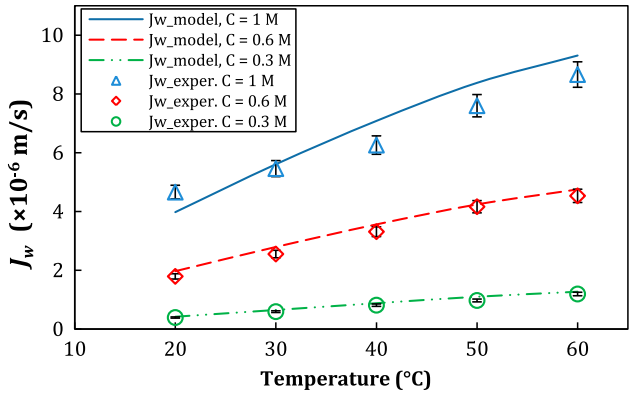

Fig. 10. Modeled (lines) and experimental results (symbols) of the water flux J_w.

6.2. Effect of the temperature on the water flux (J_w)

The water flux (J_w) at different operating conditions is now studied experimentally: three draw solutions were tested (0.3, 0.6, and 1 M of NaCl) at a range of temperatures varying from 20 to 60 ℃. The temperatures of the feed and draw solutions were held equals during the experiments. The feed solution concentration was 8.55 mM of NaCl and the applied pressure was Δp = 10. Fig. 10 shows the comparison between the experimental results and model obtained by fitting Eq. (4). Clearly, both experimental and simulated J_w increased with temperature for all the tested solutions. The experimental results are in coherence with the simulated data, except for the solution of 1 M at high temperature when the model slightly overestimates the water flux. This is probably due to the high salt flux diffusion caused by the temperature and the relatively high draw solution concentration, which decrease J_w. The 1 M solution concentration case is now studied separately.

The variation of the water flux (J_w) and the salt flux (J_s) of 1 M NaCl solution as a function of ΔP for different temperatures is presented in Fig. 11(a) and (b).

As expected, the increase in the temperature leads to the enhancement of the water flux. This result is mainly attributed to the variation of the transport parameter of the membrane due to the temperature. In fact, this increase in the water flux is caused the improvement of the water permeability of the membrane (A), which depends strongly on the temperature, the improvement of the mass transport coefficient (k), the decrease in the solute resistivity (K), and the decrease in the ECP because of the decrease in the boundary layer thickness and the increase in the mass transfer coefficient. This impact is well seen in the power density (Fig. 11(c)): at 60 ℃, the power produced is around 5.8 W/m^2 for an applied pressure of 10 bars. This value is higher than critical value that makes the PRO process commercially viable [6]. To guarantee high temperatures, the brine of thermal desalination processes satisfy this criterion (i.e. the brine temperature of a multi-effect distillation process can reach 65 ℃) [32].

Table 3
Water permeability coefficient A and salt permeability coefficient B at different temperatures

T (℃)	A (m/s/Pa)	B (m/s)
20	1.06×10^{-12}	2.62×10^{-8}
30	1.43×10^{-12}	4.25×10^{-8}
40	1.74×10^{-12}	5.87×10^{-8}
50	1.98×10^{-12}	8.00×10^{-8}
60	2.12×10^{-12}	8.80×10^{-8}

Fig. 11(b) shows the experimental variation of the salt flux (J_s) as a function of the temperature. It can be seen that the salt flux increases also when the temperature increases. This is a limiting effect to the performance of PRO, as the reverse solute diffusion induces a significant reduction in both the PRO water flux and the power density when the draw solutes diffuse through the membrane and accumulate in the porous substrate due to the water flux that has the opposite flow direction. This leads to a buildup of a draw solute concentration within the porous support layer, contributing to the increase in the ICP at the surface of the support layer, and thus, the effective osmotic pressure difference decreases.

The reverse solute diffusion occurs simultaneously with the forward water permeation in the reverse direction. A useful quantity is the specific solute flux (J_s/J_w) that describes the amount of draw solutes permeating through the membrane normalized by the volumetric water flux. The study of the ratio (J_s/J_w) at different temperatures (Fig. 11(d)) reveals that the flux ratio

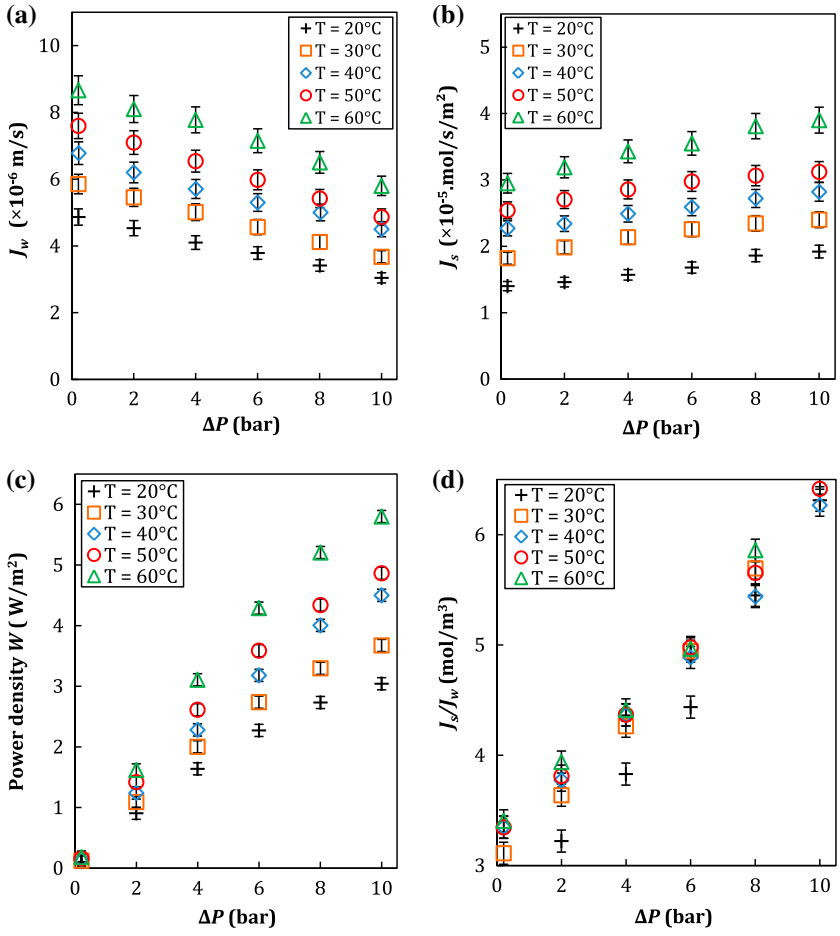

Fig. 11. Variation of the water flux J_w (a), the salt flux J_s (b), the power density W (c), and the specific solute flux J_s/J_w (d) with the temperature. $C_{D,b}$ = 1 M, $C_{F,b}$ = 8.55 mM, and u_0 = 0.0107 m/s.

increases with temperature, and it is also affected by the applied pressure. At low ΔP (<4 bars), the increase rate of the flux ratio is low compared to higher ΔP (>8 bars). In addition, the effect of the temperature is quite visible at low pressure, although this effect seems much smaller (even negligible) at $\Delta p > 8$ bars. This result shows that the temperature effect is dominated by the pressure at relatively high ΔP. Consequently, an adequate choice of the applied pressure and the temperature can be helpful to reduce the salt diffusion through the membrane.

7. Conclusions

The effect of the temperature on the PRO process has been investigated. It was shown experimentally that the temperature affects many parameters such as the diffusion coefficient, the solute resistivity, the mass transfer coefficient, and the osmotic pressure. It has been shown that, in general, working at high temperatures enhances the water flux of the process, and consequently the power recovery. The disadvantages of high temperatures are the risk of accumulation of salt at the surface of the membrane support layer, due to the fact that raising the temperature also leads to the increase in the salt reverse flux (J_s) and the degradation of the membrane. These can be overcome by the development of specific high-temperature membranes with a high resistance to reverse salt flux.

As further work, this study can be extended to real fluids (i.e. wastewater, effluents, high concentrated saline water, etc.) to investigate the effect of the matrix complexity. Moreover, the effect of the water flux J_w on the boundary layer using commercially length-scale PRO membrane can also be studied referring to the results of the current study.

Acknowledgments

This work was co-funded by the seventh framework program, under grant 288145 (H2OCean), within the Ocean of Tomorrow Joint Call 2011.

List of symbols

A — water permeability coefficient (m/s/Pa)
B — salt permeability coefficient (m/s)
$C_{D,m}$ — salt concentration of the membrane surface at the draw solution side (g/l)
$C_{F,m}$ — salt concentration on the membrane surface at the side of the feed side (g/l)
$C_{D,b}$ — salt concentration of the feed stream (g/l)
$C_{F,b}$ — salt concentration on the membrane surface at the side of the feed (g/l)
C_S — molar concentration of the solution (mol/l)
d_h — hydraulic diameter of the flow channel (m)
D — diffusion coefficient of the solution (m^2/s)
d — diameter of the pipe (m)
h_{sp} — spacer thickness (m)
J_w — water flux that crosses the membrane (m/s)
J_s — salt flux that crosses the membrane ($mol/m^2/s$)
k — mass transfer coefficient (m/s)
$k_{overall}$ — overall mass transfer coefficient (m/s)
k_x — local mass transfer coefficient (m/s)
K — solute resistivity (s/m)
k_b — Boltzman constant (–)
P_w — the hydrated perimeter (m)
ΔP — applied pressure (Pa)
$\Delta\pi$ — difference of osmotic pressure between the draw water and the feed water (Pa)
r — ion radius (m)
R — gas constant (J/mol/K)
Re — Reynolds number (–)
Re_x — local Reynolds number (–)
s — structure parameter of the support layer (m)
Sc — Schmidt number (–)
Sh — Sherwood number (–)
Sh_x — local Sherwood number (–)
S_{vsp} — specific surface of the spacer (1/m)
T_R — the normalized temperature (–)
$T_{D,b}$ — temperature of the draw water bulk (°C)
$T_{F,b}$ — temperature of the feed water bulk (°C)
u — velocity of the fluid (m/s)
V_{sp} — volume of the spacer (m^3)
η — dynamic viscosity of the solution (Pa s)
$\pi_{D,m}$ — osmotic pressure at the surface of the active layer (Pa)
$\pi_{F,m}$ — osmotic pressure at the surface of the support layer (Pa)
$\pi_{D,b}$ — osmotic pressure at the draw bulk (Pa)
$\pi_{F,b}$ — osmotic pressure at the feed bulk (Pa)
t_s — length of the support layer (m)
τ — tortuosity of the membrane (–)
ε — porosity of the membrane (–)
β — van't Hoff coefficient (–)
δ — thickness of the boundary layer (m)
ρ — density of the solution (kg/m^3)
μ_w — water kinematic viscosity (m^2/s)

References

[1] W. Guo, L. Cao, J. Xia, F.Q. Nie, W. Ma, J. Xue, Y. Song, D. Zhu, Y. Wang, L. Jiang, Energy harvesting with single-ion-selective nanopores: A concentration-gradient driven nanofluidic power source, Adv. Funct. Mater. 20 (2010) 1339–1344.
[2] X. Wang, Z. Huang, L. Li, S. Huang, E.H. Yu, K. Scott, Energy generation from osmotic pressure difference between the low and high salinity water by pressure retarded osmosis, J. Technol. Innov. Renew. Energy 1 (2012) 122–130.
[3] S. Loeb, Production of energy from concentrated brines by pressure-retarded osmosis, J. Membr. Sci. 1 (1976) 49–63.
[4] G. Han, S. Zhang, X. LiT-S. Chung, High performance thin film composite pressure retarded osmosis (PRO) membranes for renewable salinity gradient energy generation, J. Membr. Sci. 440 (2013) 108–121.
[5] S.E. Skilhagen, J.E. Dugstad, R.J. Aaberg, Osmotic power—Power production based on the osmotic pressure difference between waters with varying salt gradients, Desalination 220 (2008) 476–482.
[6] B. Simen, Ø. Skråmestø, S. Stein, E. Skilhagen, Osmotic power from prototype to industry—What will it take? in: 3rd International Conference on Ocean Energy, Bilbao, October 2010.
[7] A. Achilli, T.Y. Cath, A.E. Childress, Power generation with pressure retarded osmosis: An experimental and theoretical investigation, J. Membr. Sci. 343 (2009) 42–52.
[8] Z. Jia, B. Wang, S. Song, Y. Fan, Blue energy: Current technologies for sustainable power generation from water salinity gradient, Renew. Sust. Energy Rev. 31 (2014) 91–100.
[9] Y. Xu, X. Peng, C.Y. Tang, Q.S. Fu, S. Nie, Effect of draw solution concentration and operating conditions on forward osmosis and pressure retarded osmosis performance in a spiral wound module, J. Membr. Sci. 348 (2010) 298–309.
[10] Q. She, X. Jin, C.Y. Tang, Osmotic power production from salinity gradient resource by pressure retarded osmosis: Effects of operating conditions and reverse solute diffusion, J. Membr. Sci. 401–402 (2012) 262–273.
[11] K.-V. Peinemann, K. Gerstandt, S.E. Skilhagen, T. Thorsen, T. Holt, Membranes for power generation by pressure retarded osmosis, in: K.-V. Peinemann, S. Pereira Nunes (Eds.), Membranes for Energy Conversion, vol. 2, Wiley, Weinheim, 2008, pp. 263–273.
[12] S. Chou, R. Wang, L. Shi, Q. She, C.Y. Tang, A.G. Fane, Thin-film composite hollow fiber membranes for pressure retarded osmosis (PRO) process with high power density, J. Membr. Sci. 389 (2012) 25–33.

[13] T.Y. Cath, A.E. Childress, M. Elimelech, Forward osmosis: Principles, applications, and recent developments, J. Membr. Sci. 281 (2006) 70–87.
[14] A.R. Da Costa, A.G. Fane, D.E. Wiley, Spacer characterization and pressure drop modelling in spacer-filled channels for ultrafiltration, J. Membr. Sci. 87 (1994) 79–98.
[15] C.Y. Tang, Q. She, W.C.L. Lay, R. Wang, A.G. Fane, Coupled effects of internal concentration polarization and fouling on flux behavior of forward osmosis membranes during humic acid filtration, J. Membr. Sci. 354 (2010) 123–133.
[16] Q. She, D. Hou, J. Liu, K.H. Tan, C.Y. Tang, Effect of feed spacer induced membrane deformation on the performance of pressure retarded osmosis (PRO): Implications for PRO process operation, J. Membr. Sci. 445 (2013) 170–182.
[17] K. Touati, C. Hänel, F. Tadeo, T. Schiestel, Effect of the feed and draw solution temperatures on PRO performance: Theoretical and experimental study, Desalination 365 (2015) 182–195.
[18] S. Phuntsho, S. Hong, M. Elimelech, H.K. Shon, Osmotic equilibrium in the forward osmosis process: Modelling, experiments and implications for process performance, J. Membr. Sci. 453 (2014) 240–252.
[19] L.G. Palacin, F. Tadeo, C. Prada, K. Touati, Evaluation of the recovery of osmotic energy in desalination plants by using pressure retarded osmosis, Desalin. Water Treat. 51 (2013) 360–365.
[20] J.S. Collura, D.E. Harrison, C.J. Richards, T.K. Kole, M.R. Fisch, The effects of concentration, pressure, and temperature on the diffusion coefficient and correlation length of SDS Micelles, J. Phys. Chem. B 105 (2001) 4846–4852.
[21] S.J. You, X.H. Wang, M. Zhong, Y.-J. Zhong, C. Yu, N.Q. Ren, Temperature as a factor affecting transmembrane water flux in forward osmosis: Steady-state modeling and experimental validation, Chem. Eng. J. 198–199 (2012) 52–60.
[22] J. Kim, M. Wilf, J.S. Park, J. Brown, Boron Rejection by Reverse Osmosis Membranes: National Reconnaissance and Mechanism Study, Desalination and Water Purification Research and Development Program Report No. 127, Denver, CO: US Department of the Interior, Bureau of Reclamation, 2009, p. 22.
[23] C. Suh, S. Lee, Modeling reverse draw solute flux in forward osmosis with external concentration polarization in both sides of the draw and feed solution, J. Membr. Sci. 427 (2013) 365–374.
[24] V. Gekas, B. Hallström, Mass transfer in the membrane concentration polarization layer under turbulent cross flow, J. Membr. Sci. 30 (1987) 153–170.
[25] C.P. Koutsou, S.G. Yiantsios, A.J. Karabelas, A numerical and experimental study of mass transfer in spacer-filled channels: Effects of spacer geometrical characteristics and Schmidt number, J. Membr. Sci. 326 (2009) 234–251.
[26] J.R. Welty, C.E. Wicks, R.E. Wilson, G. Rorrer, Fundamentals of Momentum, Heat, and Mass Transfer, fourth ed., Wiley, New York, NY, 2001, pp. 554–559.
[27] M. Elimelech, S. Bhattacharjee, A novel approach for modeling concentration polarization in crossflow membrane filtration based on the equivalence of osmotic pressure model and filtration theory, J. Membr. Sci. 145 (1998) 223–241.
[28] R.W. Fox, A.T. McDonalds, P.J. Pritchard, Introduction to Fluid Mechanics, eighth ed., Wiley, Hoboken, NJ, 2011, pp. 43–60.
[29] A.H.P. Skelland, Diffusional Mass Transfer, AIChE J. 2(3) (1974) 621–1131.
[30] C.J. Geankoplis, Principles of Mass Transfer, Transport Processes and Separation Process Principles, Prentice Hall, Upper Saddle River, NJ, 2003, pp. 410–456.
[31] S. Chou, R. Wang, A.G. Fane, Robust and high performance hollow fiber membranes for energy harvesting from salinity gradients by pressure retarded osmosis, J. Membr. Sci. 448 (2013) 44–54.
[32] K. Touati, A. de la Calle, F. Tadeo, L. Roca, T. Schiestel, D.C. Alarcón-Padilla, Energy recovery using salinity differences in a multi-effect distillation system, Desalin. Water Treat. (2014) 1–8, doi: 10.1080/19443994.2014.940648.